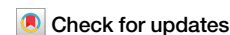


<https://doi.org/10.1038/s42003-025-07915-1>

Unmodified RNA sequences form unusual stable G-quadruplexes with potential anti-RSV and anti-angiogenesis applications



Rui-Qing Tian^{1,2,3,4,5}, Yue Gao^{1,2,5}, Xiao-Hui Hu^{1,2,5}, Meng-Hao Jia², Ling-Yun Fu^{1,2}, Di Pan^{1,2}, Sheng-Fa Su³ , Xiang-Chun Shen^{1,2} & Chao-Da Xiao^{1,2}

DNA or RNA sequences with customizable designs form unique three-dimensional structures that bind to targets with high precision and strength, making them promising tools for medical diagnosis and therapy. However, their clinical use is limited by rapid clearance from blood and safety concerns. This study introduces a novel RNA-based structure called G-quadruplex, which requires no chemical modifications. These G-quadruplexes remain highly stable in biological fluids, retaining over 90% of their concentration after 96 h. Experiments confirm their strong binding to a cell surface protein (nucleolin) without significant cellular uptake, resulting in nearly zero harm to cells. They effectively block respiratory syncytial virus infection, suppress the growth and movement of human blood vessel cells, and prevent new blood vessel formation in chicken embryos, even without specialized delivery systems. These stable G-quadruplex structures demonstrate dual potential for treating cancers and viral infections, offering a versatile and safe strategy for future therapies.

Similar to monoclonal antibodies, possessing flexible and tunable properties, nucleic acid sequences adopt the specific three-dimensional structures that significantly enhance their binding capabilities, allowing them to interact with targets with heightened selectivity and affinity. This selective binding, spanning diverse targets from small molecules to larger macromolecules like proteins or peptides, underscores the substantial potential of those nucleic acid samples for clinical translation^{1–3}. For example, the 15-nucleotide DNA oligonucleotide thrombin-binding aptamer (TBA) is tailored for binding to the thrombin protein itself⁴. 100-nt long RNA aptamers bind to organic dye⁵. Beyond their mechanistic similarity to therapeutic monoclonal antibodies, nucleic acid aptamers offer several additional advantages, including a low synthesis cost, easy modification, small molecular weight, good solubility, and negligible immune responses⁶. Thus, aptamers have garnered significant attention in the field of therapeutic agent development. Notably, a multitude of aptamers designed to target various human pathologies, including neurodegenerative diseases, age-related macular degeneration, inflammation, thrombosis, and diabetes, etc., have been developed and subjected to evaluation⁷.

Nevertheless, despite their considerable advantages, nucleic acid aptamers have encountered delays in their progression to the clinical arena. To date, only two aptamers have gained FDA approval for the treatment of age-related macular degeneration⁸. There are two main reasons attributed to its hamper for clinical application⁹. The foremost reason is their oligonucleotide nature, which often results in low stability, especially poor serum stability, thereby leading to suboptimal pharmacokinetics. For example, AS1411, extensively studied as the first aptamer evaluated in clinical trials for cancer^{10–12}, targets NCL, displaying selective cytotoxicity against cancer cells and highlighting its potential as a targeted therapeutic strategy in cancer treatment^{13,14}. However, AS1411's clinical utility was compromised by its rapid elimination from the bloodstream and relatively low potency, highlighting the importance of the stability of the sample in serum. Second, the toxicity observed in clinical trials also hampers drug development^{12,13}. Chemical modifications to safeguard nucleic acid samples from endogenous, widespread nucleases and clearance mechanisms may induce unforeseen adverse effects¹⁵. Pegnivacogin, an exceptionally promising 2'-fluoropyrimidine-modified RNA aptamer with enhanced biostability, was initially developed with high expectations for a large-scale clinical trial,

¹State Key Laboratory of Functions and Applications of Medicinal Plants, Guizhou Medical University, Guiyang, PR China. ²The High Efficacy Application of Natural Medicinal Resources Engineering Center of Guizhou Province and The High Educational Key Laboratory of Guizhou Province for Natural Medicinal Pharmacology and Druggability, School of Pharmaceutical Sciences, Guizhou Medical University, Guiyang, PR China. ³Department of Oncology, The Affiliated Hospital of Guizhou Medical University, Guizhou Medical University, Guiyang, PR China. ⁴Department of Hematology–oncology, The First People's Hospital of Guiyang, Guiyang, PR China. ⁵These authors contributed equally: Rui-Qing Tian, Yue Gao, Xiao-Hui Hu. ✉e-mail: sushengfa2005@163.com; sxc@gmc.edu.cn; xcd@gmc.edu.cn

focusing on its role as an anticoagulant with a specific target in coagulation factor IXa¹⁶. Unfortunately, the high expectations were dashed as the trial had to be prematurely terminated. In the course of the clinical trial, adverse reactions emerged. Each of these events was deemed serious, with one being life-threatening^{17,18}. This outcome underscores the critical importance of thorough safety evaluations in the development of aptamer-based therapeutics⁹. Hence, an optimal nucleic acid sample for targeted therapy should consist of natural nucleic acid sequences, ensuring both high biostability and minimal cytotoxicity.

Due to the abundance of donors and acceptors, nucleic acid sequences can form numerous intramolecular or intermolecular hydrogen bonds, resulting in the special creation of highly compact and rigid structures, including hairpin loops, i-motifs, triplexes, and more¹⁹. Furthermore, some of these structures hinder the accessibility of molecules, such as solvents or ribonucleases, to inner structural sites, thereby impeding the efficient recognition and cleavage of the nucleic acid substrate. For example, the G-quadruplex (G4), a noncanonical four-strand structure, can make it more challenging for deuterium to access and replace hydrogen atoms within the structure. This can result in reduced Hydrogen-Deuterium exchange rates²⁰. Furthermore, the specific arrangement of guanine bases in the G-tetrads may shield potential cleavage sites from enzymatic attack^{21–23}. Therefore, robust G4 structures may significantly bolster resistance to nucleases. What is particularly heartening is that recent research has revealed that specific chemical modifications not only stabilize the spatial conformation of nucleic acids, improving their chemical stability, but also offer heightened resilience against biodegradation. For instance, the strategic incorporation of 8-trifluoromethyl-2'-deoxyguanosine at specific sites in TBA enhances the formation of G-quadruplex structures with substantially higher thermodynamic stability compared to native ones. This modification results in a remarkable increase in biological stability in human plasma and a significantly enhanced anticoagulant activity²⁴. However, it's worth noting, as mentioned previously, that such modifications may increase costs and potentially lead to unforeseen toxicity. Moreover, upon conducting further structural analysis, it is believed that the binding between nucleic acids and NCL is also dependent on the formation of a G4 structure by the nucleic acid sequence, as observed in the binding between TBA, AS1411, and NCL^{13,25–28}. Thus, the identification and development of natural nucleic acid sequences with the inherent capacity to form stable G4 structures opens avenues for the design of novel biomolecules with enhanced stability and therapeutic potential.

Angiogenesis is crucial in cancer development, providing the necessary blood supply for tumor growth and enabling metastatic spread by allowing cancer cells to enter the bloodstream. Targeting angiogenesis has become an important cancer treatment strategy²⁹. Researches indicated that on the cell membrane surface, nucleolin participates in various biological processes; it was shown to shuttle between cytoplasm and cell surface and involved in cell signal transduction^{30–32}. Accumulating evidence indicates that nucleolin is transported from the nucleus to the cell membrane in endothelial cells via a unique vesicular secretory pathway, playing a crucial role in angiogenesis^{33,34}. Targeting cell surface nucleolin can interfere with key signaling pathways involved in angiogenesis, including endostatin, matrix metalloproteinases (MMPs), proto-oncogene tyrosine-protein kinase Src (SRC), focal adhesion kinase (FAK), protein kinase B (AKT), and extracellular signal-regulated kinases 1/2 (ERK1/2)^{35,36}. Recently, molecules such as peptides or aptamers that specifically bind to cell surface nucleolin have demonstrated promising anti-angiogenic effects^{37,38}.

NCL plays several important roles in respiratory syncytial virus (RSV) infection. RSV is a virus that causes severe respiratory infections, particularly common in infants and the elderly. Studies have shown that nucleolin plays the following roles in RSV infection: First, Nucleolin can act as a crucial co-factor for RSV infection. It interacts with RSV surface glycoproteins, aiding the virus in attaching to and entering host cells. Nucleolin may also be involved in the replication process of the virus within host cells, promoting the synthesis and assembly of viral RNA^{39,40}. Second, during RSV infection, nucleolin can modulate the host cell's antiviral response. It can influence

intracellular signaling pathways, regulating the host's immune response⁴¹. Given its crucial role in RSV infection, nucleolin is considered a potential therapeutic target. By designing specific small molecule inhibitors or antibodies to block the function of nucleolin, it is possible to interfere with the RSV infection process, thus achieving antiviral effects^{42,43}.

In this study, we have successfully developed a novel class of G4s formed by unmodified RNA sequences. The nuclease stability experiment revealed the remarkable resilience of these G4s, as they maintained a concentration of at least 90% post-incubation in a cell culture medium containing 10% fetal bovine serum at 37 °C for 96 h. This noteworthy resilience emphasizes the outstanding durability of these G4s, rendering them exceptionally promising for continued exploration in clinical research. MTT assays affirmed the minimal cytotoxicity of these G4s toward normal cells. Additional experimental data, encompassing surface plasmon resonance, Immunofluorescence-based flow cytometry, and confocal microscope images, validated the specific binding of G4s to cell surface NCL. Moreover, Western-blot results indicated that, in contrast to the AS1411 aptamer, these distinctive G4s do not disrupt NCL's function in regulating protein expression. This implies that G4s can modulate signal transduction at the cell surface without affecting NCL in the nucleus, thereby averting potential cytotoxicity. Furthermore, akin to other NCL binders, these G4s exhibited anti-respiratory syncytial virus (RSV) properties and effectively suppressed the proliferation, circularization, and migration of human umbilical vein endothelial cells (HUVECs). Notably, they demonstrated an anti-angiogenic effect in a chicken embryo experiment. In summary, the uniquely stable G4s presented in this study emerged as robust candidates for both tumor and RSV therapies, highlighting their versatile potential in therapeutic applications.

Results

Finding stable G-quadruplexes

Sequences that form a structure containing more than G-tetrads, such as U- or A-tetrads, consistently exhibit heightened stability, attributed to the effective enthalpic contribution of the additional tetrad⁴⁴. Furthermore, G4 formed by RNA sequences, characterized by additional hydrogen bonding and influence on molecular hydration, typically demonstrate greater stability than their DNA counterparts^{45,46}. Putative G4 sequences, with a length shorter than 12 nucleotides, demonstrate the ability to form intermolecular G4 structures. The incorporation of U or A nucleotides at the terminus of the sequences facilitates the regulation of non-G-tetrad formation, specifically U- or A-tetrad, drawing it into closer proximity to the core G-stem. Consequently, the π - π stacking interaction between the non-G-tetrad and G-tetrad elements plays a significant role in enhancing the overall stability of the entire structure. To date, telomere RNA sequences have been documented to readily form G4s with extra tetrads^{20,44,47}. Furthermore, the telomere RNA G-quadruplex exhibits structural polymorphism, adopting diverse configurations that facilitate its interaction with a multitude of proteins pivotal to various biological processes^{20,21,48–52}. It may also be capable of forming a specific G4 structure that binds to NCL¹. Consequently, we synthesized several telomeric repeat-containing RNA sequences with extended G, U, or A (Table 1). We checked the CD spectrum of those RNA sequences. The results showed that all sequences exhibited a positive peak at 265 nm and a negative peak at 240 nm in the CD spectrum, indicating that all sequences adopted parallel G4 structures (Fig. 1a)^{20,21}. Furthermore, the melting curves showed that the ORN 1, 3, 4 G4s possess high thermostability. Notably, ORN 1 and 3 demonstrated only a slight decrease in signal, even at a temperature as high as 95 °C. Similarly, ORN 4 maintained approximately one-third of its signal at 95 °C, with a T_m (melting temperature) value exceeding 70 °C, surpassing the thermostability of most G4s reported in prior literature (Fig. 1b–g). Next, nondenaturing gel showed that all sequences migrated slower than the reference DNA dT12 and some of them (ORN 2, ORN 3, ORN 4, ORN 5) moved even slower than dT24, indicating them adopting unusual higher order structure (Figs. 1h, and S1). More interestingly, in denaturing gel electrophoresis, ORN 2, ORN 3, ORN 4 showed similar mobility, which indicated that the structures formed by

Table 1 | The information of the sequences used in this study

Names	Sequence 5'-3'
ORN 1	UUAGGGU
ORN 2	GUUAGGG
ORN 3	GUUAGGGU
ORN 4	GGUUAGGGU
ORN 5	GGGUUAGGGU
ORN 6	GUUGGGGUUAG
AS1411	GGTGGTGGTGGTGTGGTGGTGGTGG
ORN 3-CY5	GUUGGGGU-CY5
ORN 4-CY5	GUUGGGGU-CY5
mutORN 3	GUUAAAAU
mutORN 4	GGUAAAAU

ORN 2, ORN 3, ORN 4 remained stable against base-pair hydrogen bond disruption by urea in denaturing condition (Fig. 1i). The unbelievable thermostability of those unique G4s encouraged us to test their biostability. Following incubation in the presence of 10% fetal bovine serum (FBS), the G4s were evaluated for their resistance to nucleases. The results revealed that the ORN 3 and ORN 4 G4s exhibited minimal change over a 6-h period, in stark contrast to AS1411, which displayed progressive degradation after only 2 h of incubation (Fig. 1j). Extended incubation revealed that the ORN 3 and ORN 4 G4s maintained over 90% stability even after 96 h (Fig. 1k–l). These results underscore the robust stability exhibited by the ORN 3 and ORN 4 G4s. To further confirm the structure formed by ORN 3 and ORN 4, NMR experiments were conducted. As shown in Fig. S2, both ORN3 and ORN 4 showed clear imino proton signals of rG residues within the G-quadruplex structure, appearing in the characteristic range of 10.0–11.5 ppm, which provides direct and definitive evidence of G-quadruplex formation by ORN 3 and ORN 4. In contrast, with A substitution of G, the mutORN 3 and mutORN 4 oligos did not^{20,21}.

ORN 3, ORN 4 G4s bind specifically to the NCL on the cell surface

Subsequently, we employed surface plasmon resonance (SPR) experiments to investigate the binding affinity between ORN 3 and ORN 4 G4s and NCL. The outcomes revealed that both ORN 3 and ORN 4 G4s displayed binding capabilities with NCL, showcasing affinity with K_d values of 5.88 ± 0.25 nM and 4.23 ± 0.12 nM, respectively. In contrast, the mutant sequence (mutORN 3 and mutORN 4) is unable to form a G4 structure and showed no binding to NCL (Fig. 2a, b and S3a, b). To validate the ability of ORN 3 and ORN 4 G4s to recognize native NCL expressed on the cell surface, we conducted a specific Immunofluorescence assay (IF). The NCL antibody was employed to detect NCL on the cell surface, and ORN 3 and ORN 4 G4s were utilized as competitors for the NCL antibody, followed with the analyzing by flow cytometry. As depicted in Figs. 2c, d and S4, ORN 3 and ORN 4 G4s exhibited effective competition with the antibody for binding to NCL both on the cell surface of Hep-2 and HUVECs. In contrast, the mutant sequence showed no discernible impact on the interaction between NCL and its corresponding antibody. This observation suggests that ORN 3 and ORN 4 G4s can indeed bind to NCL on the cell surface. Furthermore, the behavior of the mutant sequences highlights the specificity of the interactions between NCL and the G4 structures.

Given the known overexpression of NCL on the cell surface of cancerous cells and HUVECs^{34,53–55}, we proceeded to label the ORN 3 and ORN 4 G4s at the 3'-end (referred to as ORN 3-CY5 and ORN 4-CY5). This labeling aimed to assess whether these G4s could distinguish cancer cells and HUVECs from other normal cells, thereby confirming their specific binding to NCL in a cellular environment. In experiments, mixed populations of cancer and normal cells were incubated, with the proportion of cancer cells in the cell population varying. Subsequent flow cytometry analysis revealed that the fluorescence intensity of cells stained with ORN 3-CY5 and ORN

4-CY5 increased proportionally with the rising percentage of cancer cells or HUVECs, as depicted in Fig. 2e–h. These findings underscore the potential of ORN 3-CY5 and ORN 4-CY5 to specifically bind to NCL in the complex cellular milieu, suggesting their utility for distinguishing cancerous and endothelial cells from normal ones based on NCL expression levels and further confirm that the ORN 3 and ORN 4 G4s can bind to NCL in cellular environment.

Remarkably, laser confocal microscope images unveiled a notable pattern: in cancer cells, the majority of fluorescence signals were concentrated on the cell membrane, while minimal signals were observed in normal cells. In the merged group, for ORN-3 and ORN-4, red fluorescence was primarily observed in the cytoplasm, with colocalization coefficients for green fluorescence measured at 0.73 ± 0.04 and 0.84 ± 0.02 in MDA-MB468 cells and 0.76 ± 0.03 and 0.78 ± 0.02 in Hep-2 cells, respectively. In contrast, for AS1411, significant red fluorescence accumulated within the cytoplasm, and the mean colocalization coefficients decreased to 0.52 ± 0.06 and 0.27 ± 0.06 , respectively. This outcome strongly indicates that both the ORN 3 and ORN 4 G4s exhibit binding specificity to NCL on the cell surface (Figs. 3 a, b, and S5). To further corroborate this finding, we explored the impact of ORN 3 and ORN 4 G4s on the expression level of BCL-2 and P53 in treated cells using Western blot assays. Research has shown that intracellular NCL binds to the 3'-UTR of BCL-2 mRNA, enhancing its resistance to nuclease degradation. Samples targeting NCL, such as peptides and nucleic acid aptamers, can compete with NCL binding, destabilizing BCL-2 mRNA and reducing BCL-2 protein expression^{56,57}. Additionally, NCL interacts with the 5' untranslated region (5'-UTR) of p53 mRNA, thereby inhibiting its translation. Targeting NCL can upregulate p53 expression^{58,59}. Our results demonstrated that ORN 3 and ORN 4 G4s did not significantly alter the expression of the BCL-2 and p53 proteins. In contrast, AS1411, as previously reported, entered the cytoplasm and effectively suppressed BCL-2 expression and upregulated p53 expression (Figs. 3c, and S6). These collective findings suggest that the ORN 3 and ORN 4 G4s can selectively bind to NCL on the cell surface.

Given the pivotal role of NCL in cellular function, molecules that effectively bind to NCL upon entry into the cytoplasm often interfere with the function of NCL, demonstrating cytotoxic effects on cells⁶⁰. To further explore the cytotoxicity of ORN 3 and ORN 4, MTT assays were conducted across diverse cell lines, encompassing both cancerous and normal cells. Strikingly, the results unveiled a mere marginal decrease in cell viability over a 5-day period, regardless of whether cancer or normal cells were examined, even at concentrations surpassing 100 μ M for both ORN 3 and ORN 4 G4s, indicating minimal cytotoxicity. In stark contrast, the positive control, AS1411, demonstrated markedly higher cytotoxicity, with a CC_{50} value as low as 8.19 μ M, 5.32 μ M for LX-2 and Hep-2 cells, respectively (Figs. 4 and S7). These findings were consistent with laser confocal and western blot results, collectively suggesting that ORN 3 and ORN 4 G4s primarily bind to NCL located on the cell membrane without undergoing significant uptake into the cytoplasm. These findings underscore the potential of ORN 3 and ORN 4 G4s as promising candidates for further exploration in biomedical applications.

Additionally, respiratory syncytial virus (RSV) infection is known to induce the translocation of NCL from the nucleus to the cell surface^{61,62}. Next, we utilized ORN 3-CY5 and ORN 4-CY5 to monitor the changes in NCL expression on the cell surface triggered by RSV infection. Flow cytometry analysis revealed, similar to the NCL antibody, a significant increase in the fluorescence signal of cell staining by ORN 3-CY5 and ORN 4-CY5 following RSV induction (Fig. 5a–c). This data underscores the dynamic modulation of NCL expression on the cell surface in response to RSV infection, as detected by the labeled G4 probes, and again suggested the ORN 3 and 4 G4s can bind to the NCL on the cell surface.

Anti-RSV activity of ORN 3, ORN 4 G4s

The translocation of NCL to the cell surface assumes a pivotal role in viral reception, with notable viruses such as RSV demonstrating interactions with NCL on the cell surface to regulate the attachment and entry processes⁶³.

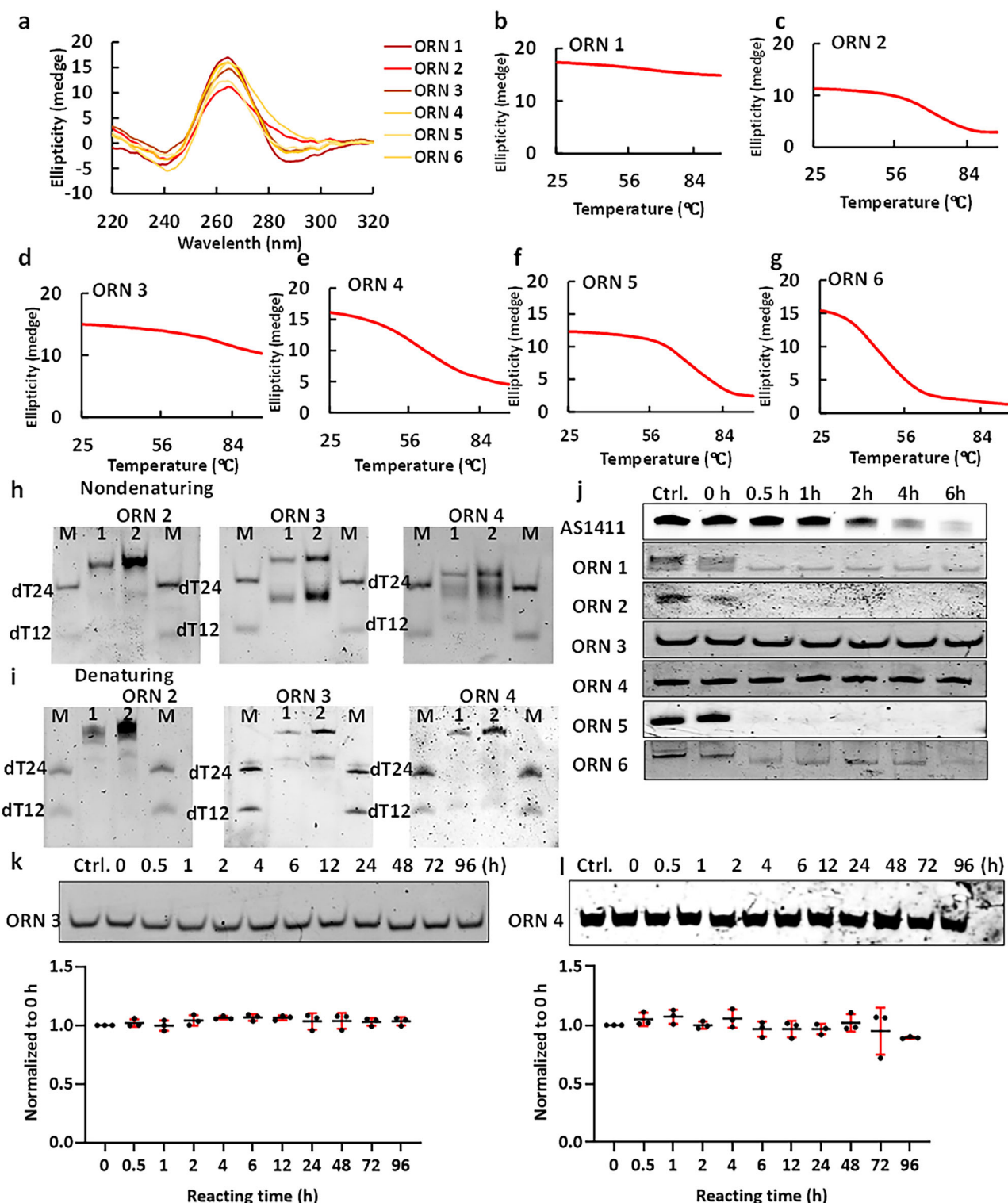


Fig. 1 | Characterization of the structural and stability properties of RNA G4s: high thermostability and nuclease resistance. **a** CD spectrum and **(b–g)** melting curve of sequences in the presence of 100 mM KCl. **h** Nondenaturing gel and **(i)**

denaturing gel of ORNs. Lane M, markers dT12 and dT24; lanes 1 and 2, ORNs (100 and 200 pmol). **j** The nuclease stable assay of sequences in 0, 0.5, 1, 2, 4, 6 h. The nuclease stable assay of **(k)** ORN 3 and **(l)** ORN 4 in 96 h.

Targeting NCL on the cell surface emerges as a potential strategy for preventing RSV infection, as evidenced by the effectiveness of agents like AS1411 and anti-NCL antibodies^{42,43}. Next, we conducted an analysis of the anti-RSV activity of ORN 3 and ORN 4 G4s. Western blot and RT-qPCR experiments were performed to investigate the expression of RSV in Hep-2 cells after a 2-h pretreatment with AS1411, ORN 3, and ORN 4 G4s. The results revealed a varying degree of reduction in the expression of the

nucleocapsid (N) gene of RSV (RSV N) the for AS1411, ORN 3 and ORN 4 G4s (Fig. 6a). Western blot analysis further showed a significant decrease in the fusion protein of RSV (RSV F protein) expression after pretreatment (Fig. 6b). In contrast, mutant samples did not exhibit similar results, indicating the anti-RSV effect of G4s at both the transcriptional and expression levels. Moreover, MTT assay in mock-infected cells was performed in parallel to comprehensively evaluate the anti-RSV activity of ORN 3 and

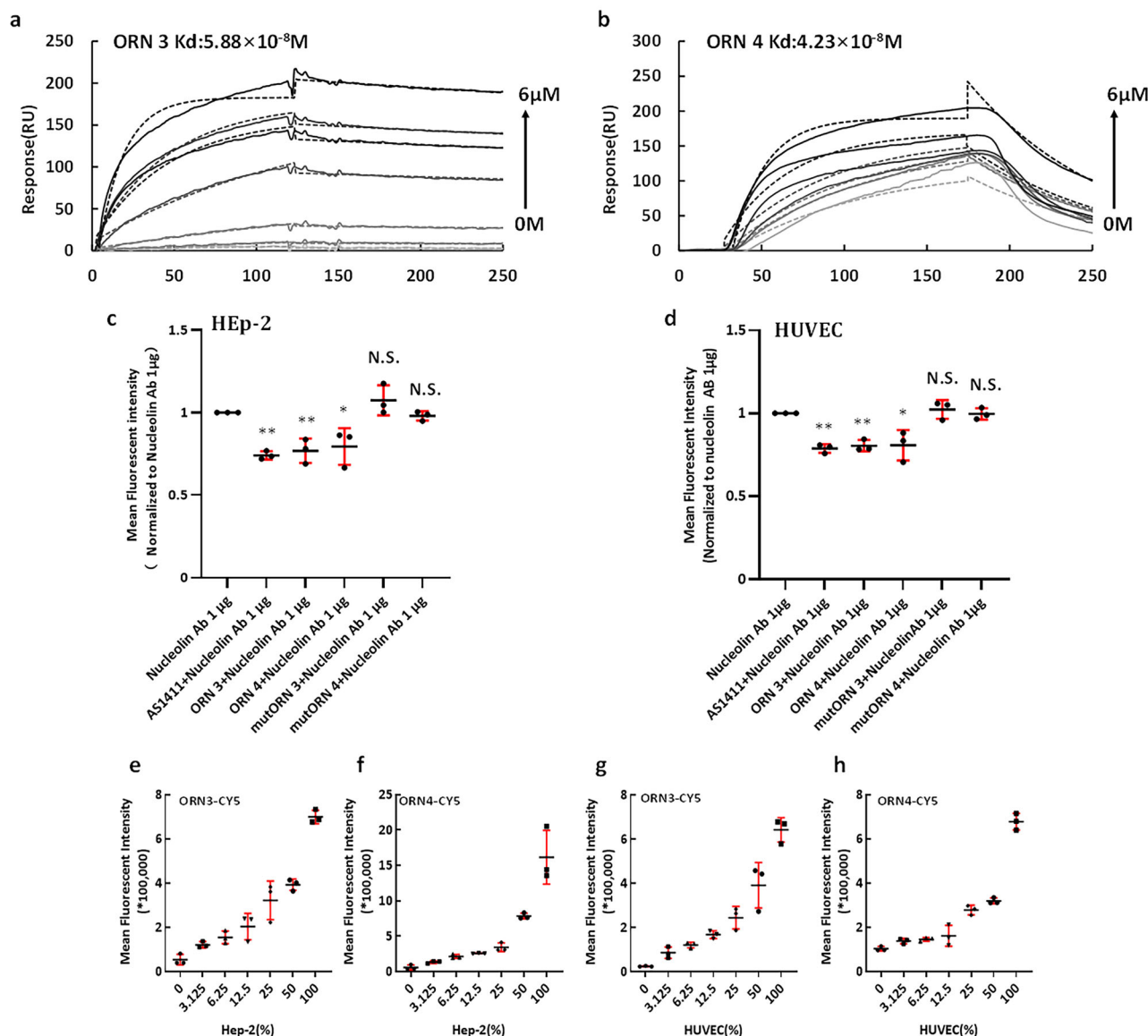


Fig. 2 | Binding affinity and cellular specificity of ORN 3 and ORN 4 G4s to NCL: SPR, immunofluorescence, and flow cytometry analysis. The sensorgrams depict the aptamer-NCL binding (resonance units vs. time) with increasing concentrations of ORN 3 (a) and ORN 4 (b) ranging from 0 μ M to 6 μ M. The mean fluorescent intensities of surface NCL on Hep-2 (c) and HUVECs (d) cells were measured using

immunofluorescence-based flow cytometry, with ORN 3 and ORN 4 serving as competitors. Furthermore, the mean fluorescence intensities of different ratios of Hep-2/LX-2 (e, f) and HUVECs/LX-2 (g, h) cells stained with ORN 3-CY5 and ORN 4-CY5 (2 μ M) were assessed, providing insights into the binding affinity of the fluorescently labeled ORNs to the cells ($n = 3$).

ORN 4 G4s. These G4s were used at a wide range of concentrations (0.78 μ M–50 μ M). In the RSV infection group, cell viability significantly decreased to ~70%. However, in the treatment group, as the concentration of ORN 3 and ORN 4 G4s increased, the viability of RSV-infected cells gradually improved in a dose-dependent manner, ultimately recovering to the level of the control group (Fig. 6c–e). These results indicate that ORN 3 and ORN 4 G4s can bind to NCL on the cell membrane, hinder the entry of RSV, and ultimately prevent RSV infection.

G4s reduced cell proliferation and migration on rhVEGF-stimulated HUVECs

NCL expressed at the cell surface is a marker of endothelial cells in angiogenic blood vessels. Targeting NCL on the cell surface has emerged as a viable strategy to impede angiogenesis. Therefore, we conducted tests to determine whether the ORN 3 and ORN 4 G4s could inhibit angiogenesis. Our initial investigation focused on assessing the impact of ORN 3 and ORN 4 G4s on cell proliferation and migration in rhVEGF-stimulated HUVECs.

Figure 7a illustrated that rhVEGF significantly enhanced HUVECs proliferation after 5 days. Interestingly, both AS1411 (used as a positive control) and various concentrations of ORN 3 or ORN 4 G4s demonstrated significant inhibition of proliferation in rhVEGF-stimulated HUVECs. In contrast, mutant samples did not exhibit similar inhibitory effects. These findings suggest that the ORN 3 and ORN 4 G4s have the potential to impede angiogenesis by specifically targeting NCL on the cell surface, thereby influencing endothelial cell proliferation in response to angiogenic stimuli.

Both wound healing and Transwell assays were employed to investigate the impact of ORN 3 and ORN 4 G4s on the migration ability of HUVECs in the presence of VEGF. The results demonstrated that ORN 3 and ORN 4 G4s exerted a concentration-dependent inhibition of HUVECs migration stimulated by rhVEGF. Similarly, AS1411, used as a positive control, also exhibited inhibitory effects on the migration of HUVECs stimulated by rhVEGF. In contrast, mutant samples did not show similar inhibitory effects (Fig. 7b, c). Western blot analysis further revealed that the

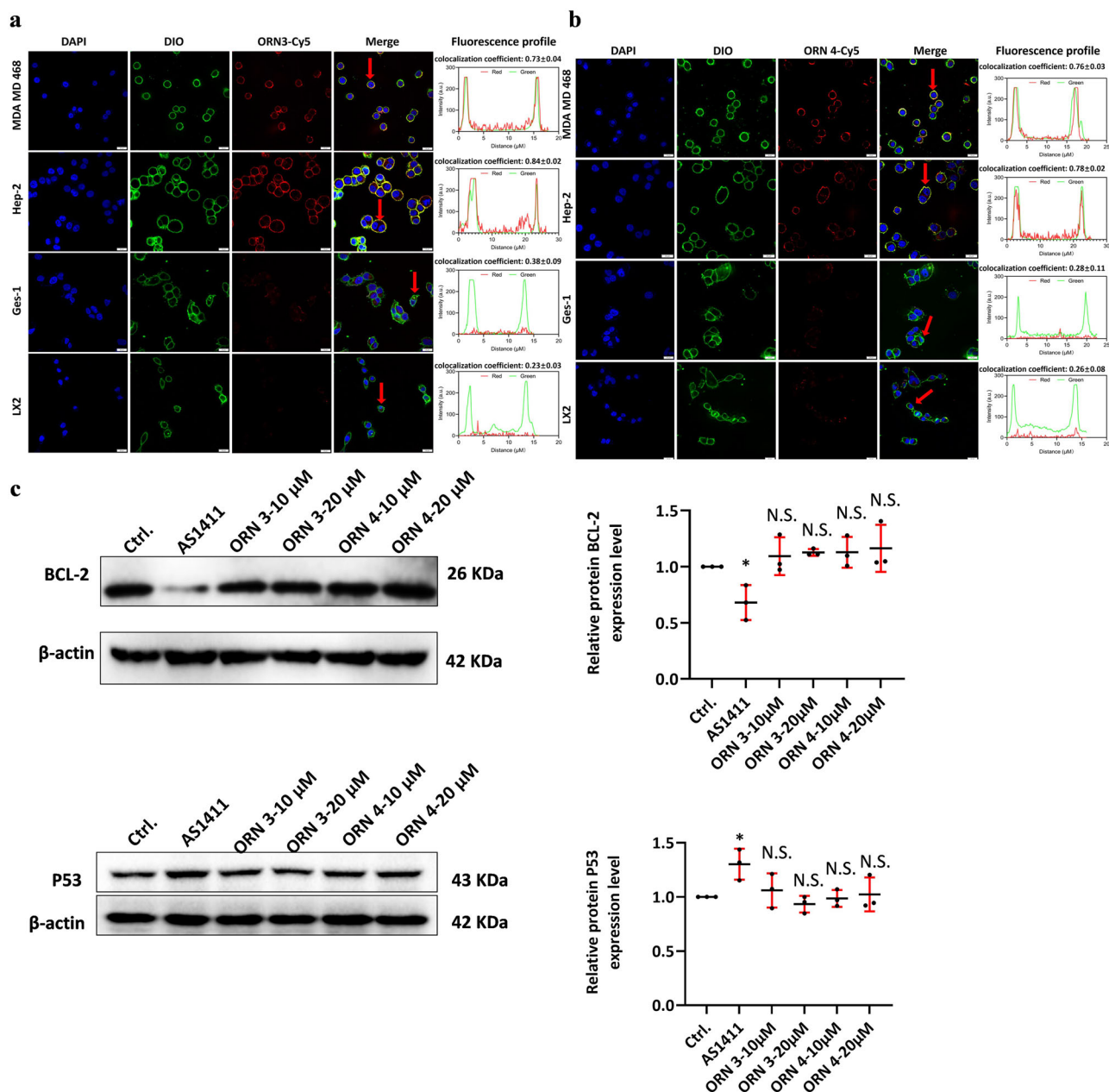


Fig. 3 | Cellular localization and functional impact of ORN 3 and ORN 4 G4s: confocal microscopy and western blot analysis. Laser confocal microscope images of cancer (Hep-2, MDA MB 468) and normal cells (Ges-1, LX-2) treated with (a) ORN 3-CY5 (2 μM) and (b) ORN 4-CY5 (2 μM). Scale bar: 20 μm. Green channel: $\lambda_{\text{ex}} = 488 \text{ nm}$, $\lambda_{\text{em}} = 500\text{--}530 \text{ nm}$. Blue channel: $\lambda_{\text{ex}} = 405 \text{ nm}$, $\lambda_{\text{em}} = 440\text{--}470 \text{ nm}$.

Red channel: $\lambda_{\text{ex}} = 561 \text{ nm}$, $\lambda_{\text{em}} = 600\text{--}700 \text{ nm}$. c Western blot analysis of BCL-2 and P53 protein expression in Hep-2 treated with ORN 3, ORN 4 (low dose 10 μM, high dose 20 μM), and AS1411 (10 μM). (* $P < 0.01$, AS1411 with control; N.S. (nonsignificant) = $P > 0.05$ $n = 3$).

HUVECs migration was primarily achieved indicating by down-regulating the expression levels of matrix metalloproteinase-2 (MMP-2) and matrix metalloproteinase-9 (MMP-9) in HUVECs, which are the angiogenesis marker proteins that play important roles in degradation and remodeling of the extracellular matrix and essential for angiogenesis (Fig. S8a, b). These findings provided mechanistic insights into the anti-angiogenic effects of ORN 3 and ORN 4 G4s, suggesting a potential role in modulating key factors involved in endothelial cell migration.

G4s inhibited tube formation on rhVEGF-stimulated HUVECs

To further explore the anti-angiogenic activity of ORN 3 and ORN 4 G4s, HUVECs were inoculated on 96-well plates coated with Matrigel for 8 h, followed by the addition of 10 ng/mL VEGF as a positive control. The results revealed that rhVEGF promoted the HUVECs Tube formation, while both

AS1411 and ORN 3, ORN 4 G4s reversed this effect, demonstrating inhibitory effects on angiogenesis. However, mutant samples were unable to inhibit the HUVECs Tube formation stimulated by rhVEGF (Fig. 8a). Moreover, western blot analysis confirmed that additional VEGF up-regulated the expression level of VE-cadherin in HUVECs, which is also the key protein for angiogenesis, and this biological activity was counteracted by ORN 3 and ORN 4 G4s (Fig. 8b). These results provide additional evidence supporting the anti-angiogenic potential of ORN 3 and ORN 4 G4s, highlighting their ability to modulate key factors involved in angiogenesis.

Anti-angiogenic effect of ORN 3 and ORN 4 G4s

In the final, we validated the anti-angiogenic effects of ORN 3 and ORN 4 G4s using a chorioallantoic membrane (CAM) angiogenic model. Serving as a positive control, AS1411 exhibited a significant impairment in the

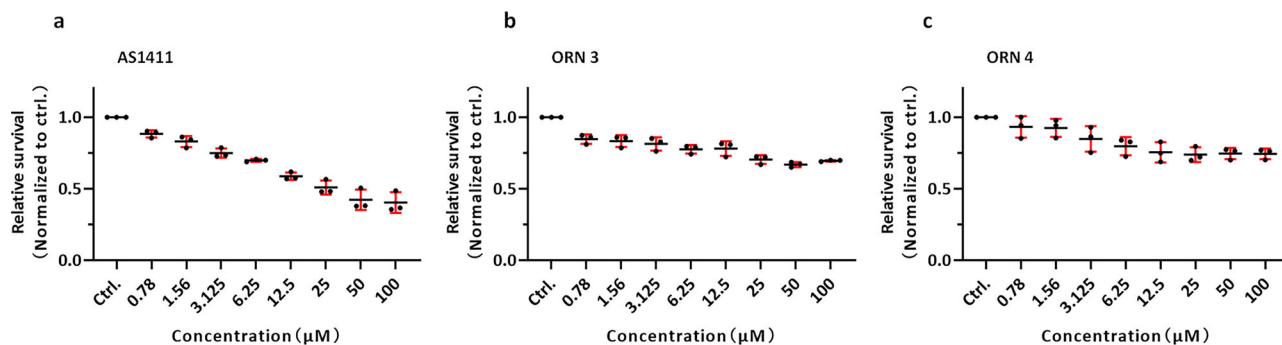


Fig. 4 | Cytotoxicity evaluation of ORN 3 and ORN 4 G4s. **a** AS1411 (0–100 μM) Toxicity to LX-2 cells, treatment time 5 days. **b** ORN 3 (0–100 μM) Toxicity to LX-2 cells, treatment time 5 days. **c** ORN 4 (0–100 μM) Toxicity to LX-2 cells, treatment time 5 days ($n = 3$).

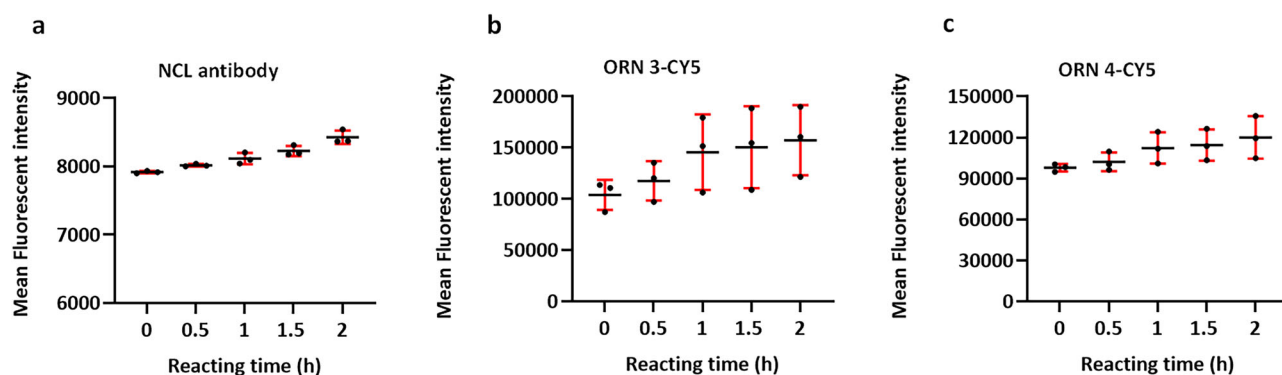


Fig. 5 | Monitoring NCL expression on the cell surface in response to RSV infection using ORN 3-CY5 and ORN 4-CY5. **a** NCL antibody (1:100) **b** ORN 3-CY5 (2 μM) and **c** ORN 4-CY5 (2 μM) monitoring the NCL changes RSV induced on cell membrane ($n = 3$).

branching and development of blood vessels, consistent with findings reported in the literature³⁷. Similarly, both ORN 3 and ORN 4 G4s demonstrated a remarkable inhibition of blood vessel branching and development, further affirming their potent anti-angiogenic effects (Fig. 9). These conclusive results underscore the robust anti-angiogenic activity of ORN 3 and ORN 4 G4s, highlighting their potential as promising candidates for therapeutic interventions targeting angiogenesis-related disorders.

Discussion

The increasing number of approved nucleic acid therapeutics underscores their potential as viable treatments for various diseases⁶⁴. The highly flexible nature of nucleic acid sequences allows them to form specific three-dimensional structures, facilitating direct molecular targeting by binding to specific targets. However, due to the intrinsic complexity of target structures, research efforts often prioritize the extensive screening of active binding molecules targeting specific sites, sometimes overlooking the inherent three-dimensional structures formed by the molecules themselves.

In this study, our research focused on NCL, a protein known for its specific binding to nucleic acids that adopt G4 structures. We aimed to identify nucleic acid sequences capable of forming robust G4 structures, as such resilience could enhance NCL binding and improve resistance to nuclease degradation in serum. Notably, natural telomere RNA sequences form highly stable G4 structures, which can interact with cell surface-expressed NCL and maintain their integrity in serum. Previous studies have shown that G-quadruplex-based aptamers, such as AS1411, formed by other sequences, possess anti-RSV and anti-angiogenesis activity. These sequences also bind to NCL, a key target for these therapeutic strategies. Since telomere RNA is rich in guanines, it is capable of forming multiple G4 conformations. Therefore, it is highly likely that the G4 structures formed by telomere RNA sequences may also exhibit anti-RSV and anti-angiogenesis activities. This suggests promising applications in developing NCL-targeted

therapies against diseases such as RSV infections and angiogenesis-related conditions.

Although most ORNs that exhibit high thermostability are correlated with high biostability in serum, ORN 1, despite its high T_m value and ability to maintain a highly ordered structure under denaturing conditions, is quickly digested in serum. This discrepancy may be due to ORN 1 forming rigid structures similar to ORNs 3 and 4, which inhibit molecules from accessing the inner core of the nucleic acid structure, making them resistant to urea. However, ORN 1 may contain specific recognition sites on the external side of its G-quadruplex for nucleases, leading to its rapid digestion. A detailed structural study to uncover these differences would help address this question. Nucleases degrade nucleic acids by recognizing specific 3D conformations, particularly in the case of ORNs 3 and 4. The sequence of the G4 loop plays a crucial role in influencing the stability of G-quadruplex structures, with aberrant base pairing within the loop enhancing this stability. The resistance of ORN 3 and ORN 4 G-quadruplexes to nucleases may be attributed to their atypical loop folding. Our previous study also showed that telomeric G4s, analogous to ORNs 3 and 4, bind to surface NCL without internalizing into the cytoplasm¹. This suggests that such G4s may possess comparable topological features that interfere with endocytosis. However, the high biostability observed in ORNs 3 and 4 suggests that they differ from these analogs. A comprehensive structural investigation to elucidate these variances would offer valuable insights into the mechanisms governing nuclease binding and endocytosis. Aptamer entry into cells via endocytosis is influenced by factors such as size, stability, and structure. ORN 3 and ORN 4 may fail to penetrate membranes due to their unique conformations. Their slower migration speed compared to dT24 suggests the formation of larger G-quadruplex structures. These structures are stabilized by cation coordination and ionic strength, but the cell membrane's selective barrier poses a challenge for charged molecules like ORN 3 and ORN 4 G-quadruplexes. However, the difficulty in internalizing these

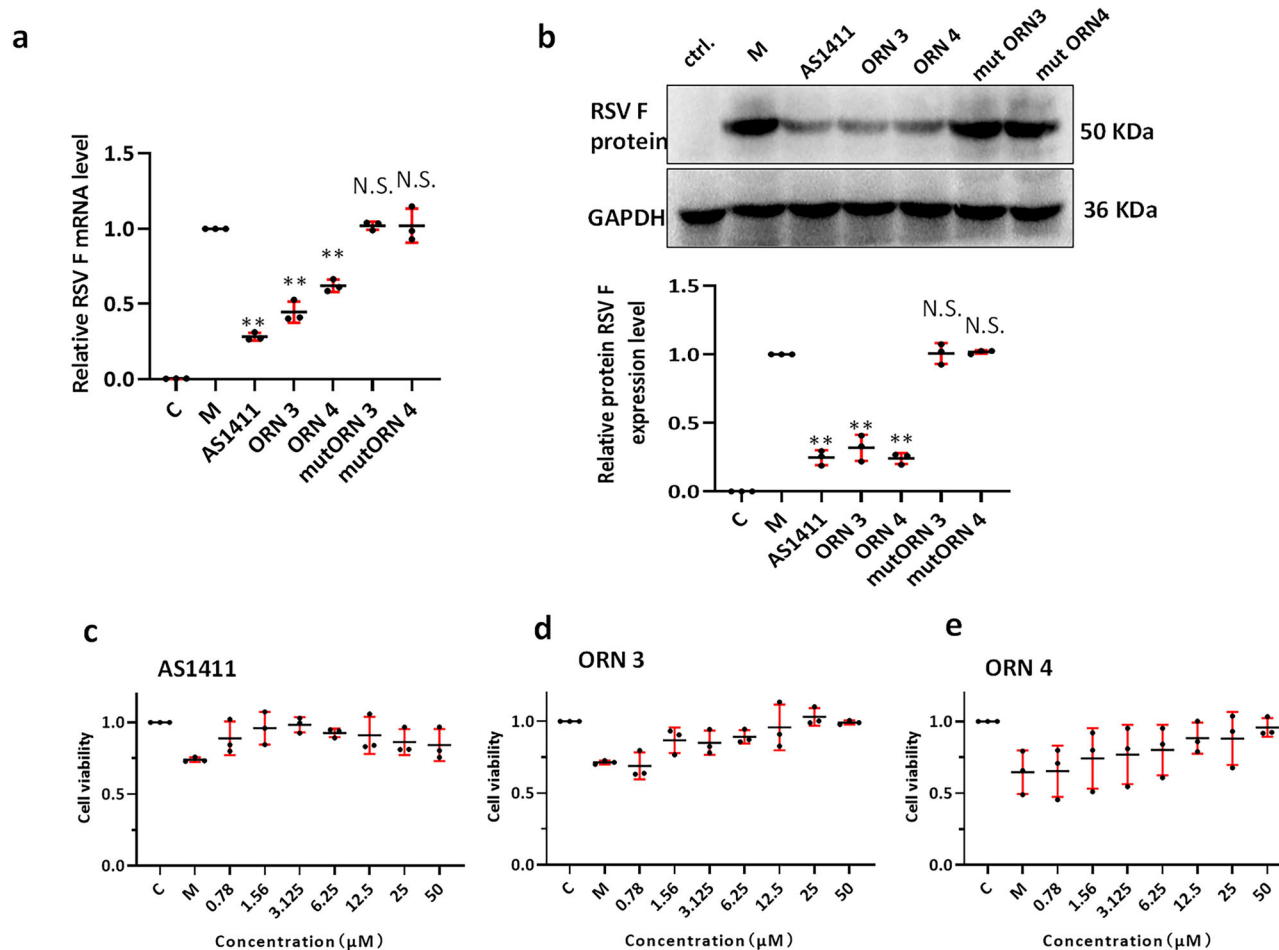


Fig. 6 | Anti-RSV activity of ORN 3 and ORN 4 G4s: targeting NCL on the cell surface. **a** RT-qPCR analyzed the RSV N mRNA transcription levels after different treatments by AS1411, ORN 3, and ORN 4 (10 μ M). Line M, RSV-infected model.

Line C, control ($n = 3$) (b) RSV F protein expression levels were detected by western blot ($n = 3$). The anti-RSV effect of different concentrations of (c) AS1411, (d) ORN 3, and (e) ORN 4. ** $P < 0.01$ vs. control group (Student's t -test) ($n = 3$).

aptamers, ORN 3 and ORN 4 G-quadruplexes, may relate to their structures and the fact that they carry more ions, which hinders their passage through the cell membranes. Since ORNs 3 and 4 can target both cancer cells and HUVECs, potential delivery methods like nanoparticles with different sizes, which can be passively enriched in tumor tissues through the EPR effect, may better enable their combined anticancer efficacy.

Methods

Oligonucleotide synthesis and sample preparation

Oligonucleotides were synthesized on a 1 μ mol scale using an automated DNA/RNA synthesizer (NTS, Japan). Following synthesis, the oligonucleotides were detached from the support and deprotected. Purification of the oligonucleotides was carried out via High-Performance Liquid Chromatography (HPLC) (Shimadzu, China). Subsequently, desalting was performed using a NAP-10 column (GE Healthcare, USA). The G4 sample preparation involved a solution containing 100 mM KCl and 10 mM K_3PO_4 (pH 7.0). The samples were subjected to heating at 95 $^{\circ}C$ for 5 min, followed by natural cooling to room temperature.

Non-denaturing gel electrophoresis and denaturing gel electrophoresis

Non-denaturing gel electrophoresis was conducted using 20% (19:1) polyacrylamide gels. For denaturing gel electrophoresis, 8 M urea was incorporated into the 20% (19:1) polyacrylamide gels. The gel was stained with GelStarTM.

Nuclease stability assay

A 10 μ L aliquot of the G4 samples was incubated with an equal volume of medium containing fetal bovine serum at 37 $^{\circ}C$ for various durations ranging from 0 to 96 h. Subsequently, 1.5 times the volume of 10 M urea was added to the incubation mixture. The entire sample was then denatured at 100 $^{\circ}C$ for 5 min and subsequently stored at $-20^{\circ}C$. Electrophoresis of the samples was performed on 20% denaturing polyacrylamide gels, and the resulting bands were visualized using GelStarTM staining.

Circular dichroism (CD) analyzes

The CD spectrum was acquired using a circular dichroism spectrophotometer (JASCO, Japan). The G4 samples, comprising a nucleic acid concentration of 10 μ M in a buffer containing 100 mM KCl and 10 mM K_3PO_4 (pH 7.0), were denatured at 95 $^{\circ}C$ for 5 min, followed by natural cooling to room temperature overnight at 4 $^{\circ}C$. Circular dichroism measurements were performed at 25 $^{\circ}C$ with a wavelength range of 220–320 nm at a scanning speed of 100 nm/min, using K_3PO_4 buffer as a blank control.

G4 Samples were subjected to a temperature ramp from 25 $^{\circ}C$ to 95 $^{\circ}C$ at a rate of 1 $^{\circ}C$ /min, and the CD signal at the maximum positive absorption peak was monitored in real-time. Data was collected for every 1 $^{\circ}C$ increase in temperature, and the melting curve was plotted using temperature as the x -axis and normalized CD signal values as the y -axis. The temperature at which the CD signal value decreased to half of its maximum was defined as the melting temperature (T_m).

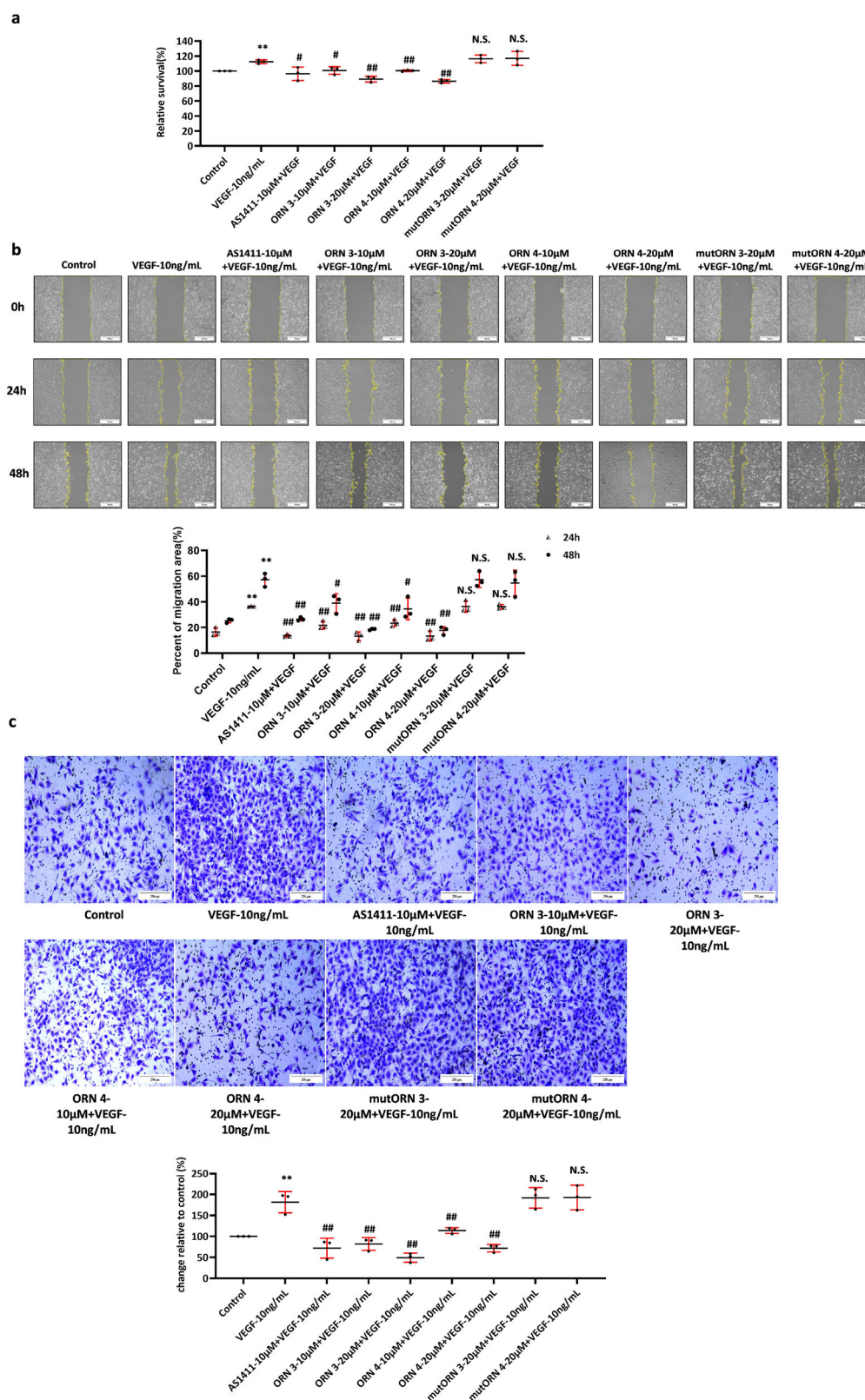
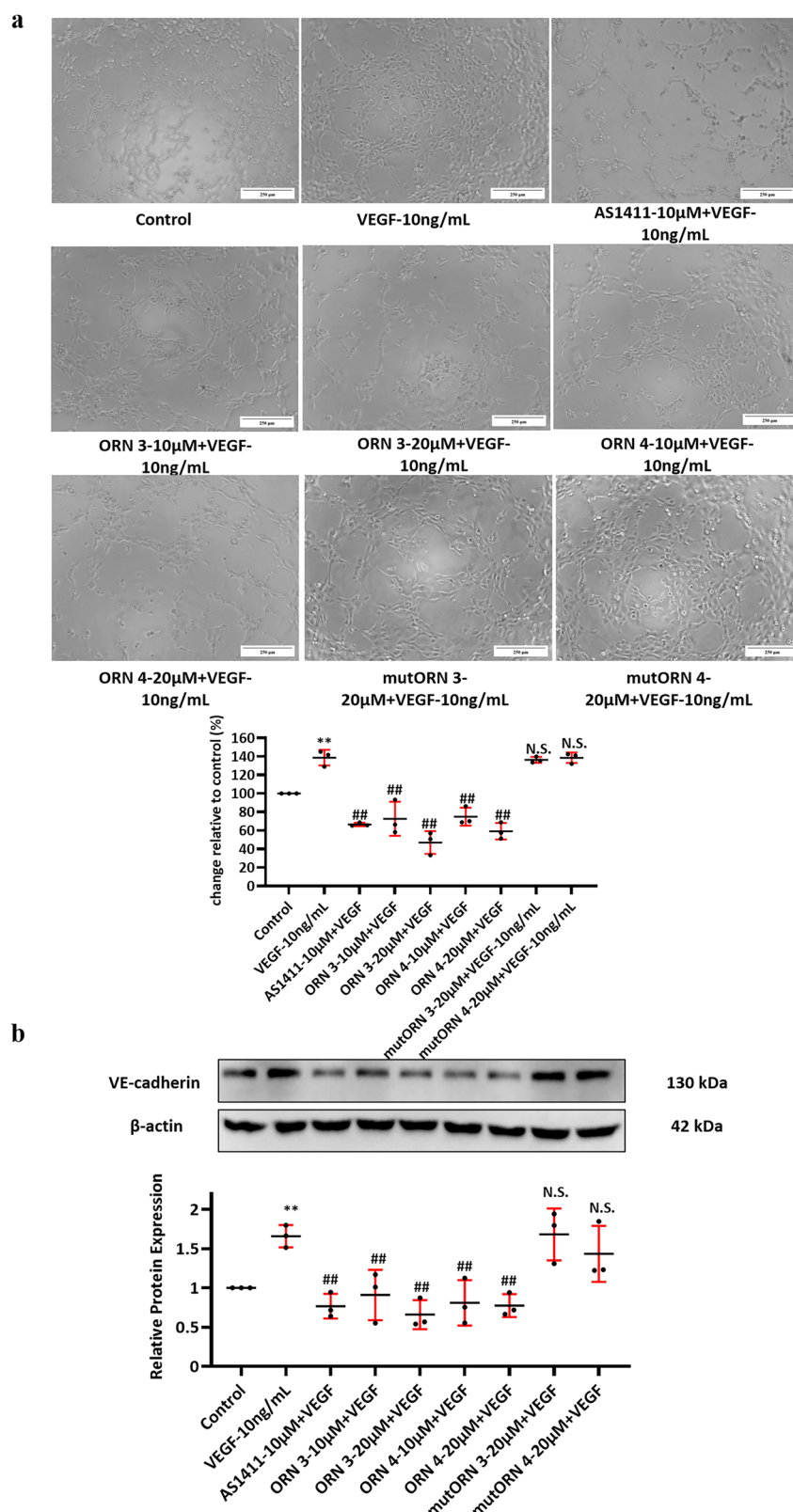


Fig. 7 | Inhibition of rhVEGF-induced HUVEC proliferation by ORN 3 and ORN 4 G4s. a Anti-proliferation effect of ORN 3 and ORN 4 G4s on HUVECs stimulated by VEGF ($n = 3$). **b** Wound healing assay analyzed the effects of ORN 3 and ORN 4 G4s on HUVECs migration stimulated by VEGF. Scale bar: 250 μ m ($n = 3$).

c Transwell assay analyzed the effects of ORN 3 and ORN 4 G4s on HUVECs migration stimulated by VEGF. Scale bar: 250 μ m. ** $P < 0.01$ vs. control group; ## $P < 0.01$ vs. VEGF group (Student's t -test) ($n = 3$).

Fig. 8 | Anti-angiogenic activity of ORN 3 and ORN 4 G4s: inhibition of HUVEC tube formation and modulation of VE-cadherin expression. a

ORN 3 and ORN 4 G4s inhibited the tube formation of HUVECs stimulated by VEGF. Scale bar: 250 μ m ($n = 3$). **b** Western blot analyzed of VE-cadherin protein expression in HUVECs stimulated by VEGF and treated with ORN 3 and ORN 4 G4s (low dose 10 μ M, high dose 20 μ M), AS1411 (10 μ M), mutORN 3, mutORN 4 (20 μ M). ** $P < 0.01$ vs. control group; ## $P < 0.01$ vs. VEGF group (Student's t -test) ($n = 3$).



Surface plasmon resonance

The Surface Plasmon Resonance (SPR) experiments were carried out using a Biacore T200 instrument (Cytiva, USA). In a concise overview, carboxyl groups on the surfaces of the Fc3 and Fc4 channels of the chip were activated by employing 0.4 M EDC and 0.1 M NHS. This activation process involved a contact time of 400 s and an injection flow rate of

10 μ L/min. Following activation, NCL was coupled to the Fc4 channel using a pH 4.0 sodium acetate coupling buffer at a concentration of 25 μ g/mL. The coupling step had a contact time of 420 s and a flow rate of 10 μ L/min. Subsequently, the Fc3 and Fc4 channels were sealed with 1 M ethanolamine, employing a contact time of 400 s and a flow rate of 10 μ L/min.

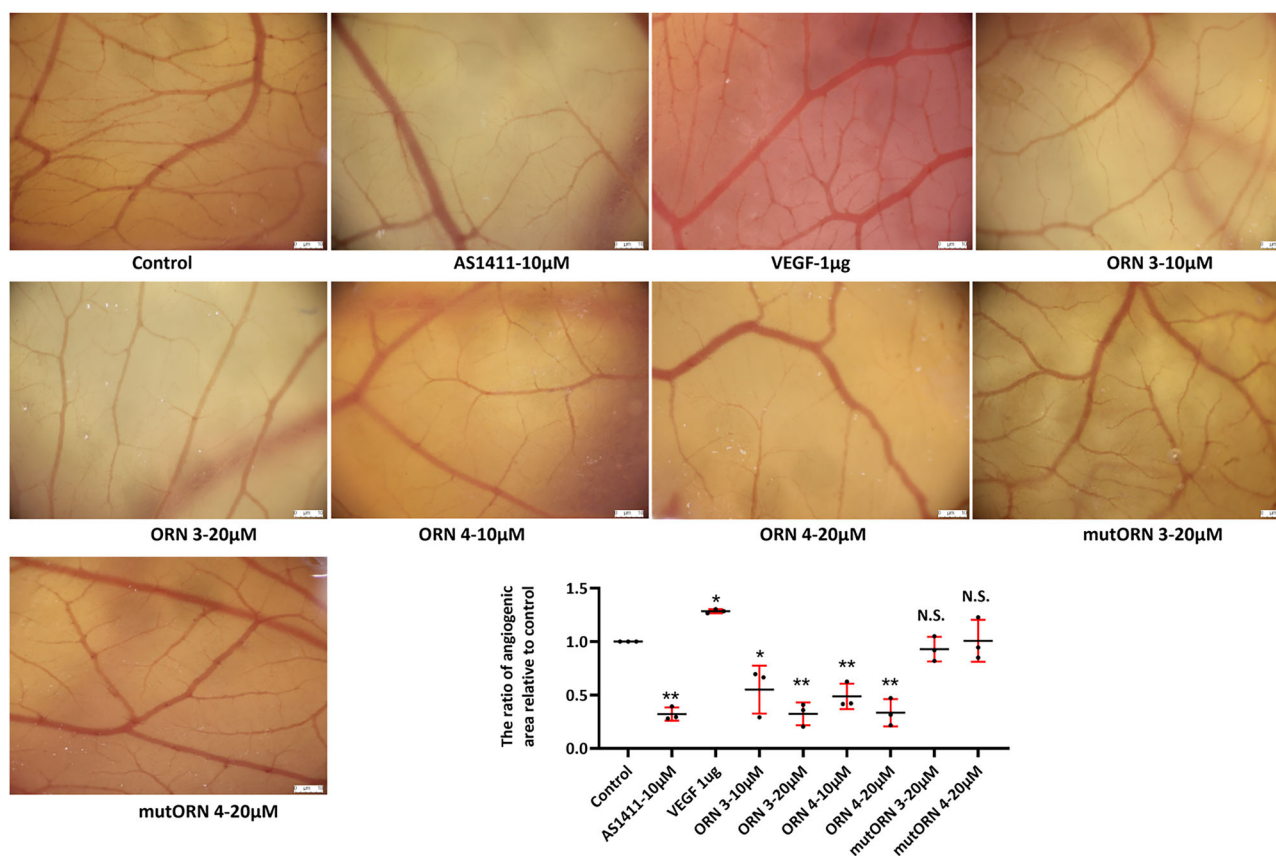


Fig. 9 | Validation of anti-angiogenic effects of ORN 3 and ORN 4 G4s. Inhibition of angiogenesis by ORN 3 and ORN 4 G4s in chick embryo chorioallantoic membrane (CAM) assay. Scale bar: 10 μ m. ** P < 0.01 (Student's t -test) (n = 3).

In the context of interaction studies, G4 samples with varied concentrations of nucleic acid were sequentially injected. The injection process involved a contact time of 120 s or 180 s, followed by a dissociation time of 250 s or 300 s. Regeneration steps with 1 M KCl were implemented between each concentration injection. Changes in response signal values were recorded throughout the experiments.

Cell culture and cell viability assay

We obtained Hep-2 (CCL-23), MDA MB 468 (HTB-132), MCF-7 (HTB-22), and Vero cell lines (CCL-81) from ATCC. HL7702 (BNCC338358), Ges-1 (BNCC337969), and LX2 (BNCC337957) cells were purchased from BNCC. All cell lines were cultured in DMEM supplemented with 10% FBS, 100 U/mL penicillin, and 100 μ g/mL streptomycin and maintained at 37 °C in a 5% CO₂ incubator.

HUVECs (CTCC-0804-PC) were procured from Shanghai Sainuo Biotechnology and cultured in 5% CO₂ at 37 °C with 5% fetal bovine serum (Gibco, USA), 100 U/mL penicillin, 100 μ g/mL streptomycin, and 1% endothelial cell growth additive (ECGS).

For the cell viability assays, Hep-2, MDA MB 468, Hela, MCF-7, HL7702, LX-2, and Ges-1 cells were seeded at a density of 3×10^4 cells per well in 96-well plates and allowed to grow overnight. The following day, the cells were exposed to varying concentrations of G4 samples (0–100 μ M) for a period of 5 days. To perform the MTT assay, 15 μ L of MTT (5 mg/mL) was added to each well, and the plates were incubated for 4–6 h. Formazan crystals were then dissolved in 150 μ L of DMSO, and the absorbance was measured at 490 nm using a BioTek spectrophotometer (USA). The experiment was conducted in triplicate.

Antibodies and reagents

Antibodies against BCL-2 (26593-1-AP, 1:1000 dilution), MMP-9 (10375-2-AP, 1:1000 dilution), MMP-2 (10373-2-AP 1:1000 dilution) and β -Actin

(81115-1-RR, 1:10000 dilution) were purchased from ProteinTech Group, Inc. Antibodies against VE-cadherin (ab313632, 1:1000 dilution), NCL (ab22758, 1:100 dilution) were purchased from Abcam. Horseradish peroxidase (HRP)-conjugated goat anti-rabbit IgG (A0208, 1:10,000 dilution) and HRP-conjugated mouse IgG (A0216, 1:10,000 dilution) were purchased from Beyotime Institute of Biotechnology. Recombinant human VEGF (VEGF165) was obtained from R&D Systems (USA). Matrigel was purchased from BD Biosciences (USA). Respiratory syncytial virus antibody (2F7) (sc-101362, 1:1000 dilution) was purchased from SANTA CRUZ (USA).

IF-based flow cytometry for assessing aptamer binding to cell surface nucleolin

The adherent cells were detached using 2 mM EDTA, pre-treated with 2 μ M G4 samples at 4 °C for half an hour, and followed by three washes with cold phosphate buffer. Subsequently, the cells were incubated with varying concentrations of anti-NCL antibody at 4 °C for 1 h. After centrifugation, the cells were washed three times with cold phosphate buffer and then incubated with Alexa Fluor 488-labeled goat anti-rabbit IgG (H + L) (Beyotime, A0423, 1:200 dilution) at room temperature for 1 h. Following another round of centrifugation and three washes with cold phosphate buffer, flow cytometry (ACEA Biosciences, USA) detection was performed.

Recognition between normal cells and cancer cell and detection of RSV infection by flow cytometry

Hep-2, HUVECs and LX-2 were inoculated in culture plates at different ratios 12–16 h, later incubated with 2 μ M CY5 labeled G4 samples for 1 h at 37 °C. Then, the fluorescence intensity was detected by flow cytometry.

Vero were seeded in culture plates overnight growth, then adsorbed 1 h by RSV (MOI 0.01). After that, 2% fetal bovine serum culture medium at

various periods. Later incubated with 2 μ M CY5 labeled G4 samples for 1 h at 37 °C. Then the fluorescence intensity was detected by flow cytometry.

Laser confocal microscope images of cells treated with G4 samples

The cells were cultured in optimal equipment for 12–16 h, followed by incubation at 37 °C with CY5 labeled G4 samples for 1 h, washing three times with PBS, fixing at room temperature with 4% paraformaldehyde for 20 min, staining with DAPI (BD5010, Bioworld, USA) for 10 min, and staining with DIO (C1993S, Beyotime, China) 37 °C for 20 min. G4 samples to cell binding image acquisition obtained through laser confocal microscopy (Olympus VS200 confocal microscope, Japan). Confocal images were acquired using a laser confocal microscope to obtain overlay images, which were then split into individual channels for DIO (green) and CY5 (red). Colocalization analysis was using ImageJ software, and the Pearson's correlation coefficient was calculated. The experiment was repeated three times, and statistical analysis was conducted.

Western blot

The cells treated with G4 samples were lysed using RIPA cleavage buffer containing 1 mM benzenesulfonyl fluoride (Beyotime, China). The protein concentration in the lysates was determined using a BCA protein analysis kit (Beyotime, China). Subsequently, total protein (50–60 μ g) was separated by SDS-PAGE gel and transferred to a PVDF membrane (Millipore, USA). The membrane was blocked with 5% skim milk at room temperature for 2 h and then incubated overnight with a primary antibody at 4 °C, following the manufacturer's instructions. Afterward, the membrane was incubated with the secondary antibody, either HRP-conjugated Affinipure Goat Anti-Mouse IgG(H + L) or HRP-conjugated Affinipure Goat Anti-Rabbit IgG(H + L). Finally, the membrane was treated with an NcmECL ultra-hypersensitive chemiluminescence reagent (NCM Biotech, P10300). The resulting spots were scanned using a ChemiDoc™ XRS system (BIORAD, USA) and analyzed using Image Lab (BIORAD).

Statistics and reproducibility

All experimental data were expressed as the mean \pm SEM of at least three independent experiments. All data fitting and statistical analyzes were carried out using GraphPad Prism software or Microsoft Excel. Statistical analysis was carried out using the student's *t*-test when analyzed with the control group. Nonsignificant was defined as $p > 0.05$, the level of significance was defined as * $p < 0.05$, and the level of highly statistical significance was defined as ** $p < 0.01$.

Quantitative real-time polymerase chain reaction (RT-qPCR)

Hep-2 cells were pre-treated with G4 samples for 2 h, followed by infection with RSV (MOI 0.01). After 48 h, total RNA extraction was performed using RNA-easy Isolation Reagent (R701-01, Vazyme, China). Reverse transcription was carried out using the EasyScript® One-Step gDNA Removal and cDNA Synthesis SuperMix (AE311-02, Trans Gen Biotech, China). The RSV mRNA level was then estimated following the manufacturer's spin protocol.

The PCR reaction parameters included an initial denaturation at 94 °C for 10 min, followed by 40 cycles of denaturation at 94 °C for 5 s, annealing at 64 °C for 30 s, and extension at 72 °C for 20 s. GAPDH was used as an internal reference gene, and the relative expression level of target genes was calculated using the double delta Ct ($\Delta\Delta$ Ct) method. The primers used were as follows: RSV N (Forward: AAGGCTTACTACCCAAGGAT, Reverse: GGATCTTTAGGTGATGTGA) and GAPDH (Forward: CAGGAGG-CATTGCTGATGAT, Reverse: GAAGGCTGGGGCTCATTT).

Wound-healing assay

HUVECs were seeded in 6-well plates and allowed to reach 90% confluence. Subsequently, a wound line was created using a 200 μ L plastic pipette tip. The cells were then incubated in serum-free ECM medium with or without VEGF (10 ng/mL) and exposed to G4 samples at low dose (10 μ M) or high

dose (20 μ M), mut samples (20 μ M), and AS1411 (10 μ M). The wound-healing process was documented at time points 0, 24, and 48 h, and the cell migration area was quantified by analyzing the images.

Migration assay

A Transwell cell migration system (8- μ m, BD Falcon, USA) was used to perform the cell migration assays. HUVECs (2×10^4 /well) were added to the upper chamber of a Transwell plate, and 500 μ L of serum-free medium with or without VEGF (10 ng/mL) and G4 samples (low dose 10 μ M/high dose 20 μ M), mut samples (20 μ M) and AS1411 (10 μ M) was added to the lower chamber. After 48 h of incubation, the migrated cells were fixed with 95% methanol and stained with 0.1% crystal violet for 30 min followed by washing 5 times with PBS.

Cell proliferation assay

HUVECs (3×10^3 /well) were seeded in six 96-well plates. Once the cells were attached, 1% ECM with or without VEGF (10 ng/mL) and G4 samples at low dose (10 μ M) or high dose (20 μ M), mut samples (20 μ M), and AS1411 (10 μ M) were added to replace the plate supernatant. The culture plates were labeled and incubated at 37 °C under 5% CO₂. After 5 days, 15 μ L of 5 mg/mL MTT was added for 4–8 h. The medium was then discarded, and 150 μ L DMSO was added to each well. After complete dissolution of the formazan, the absorbance (OD) was measured at 490 nm using a Varioskan LUX microporous plate detector (Thermo Fisher, USA). The experiment was repeated three times.

Tube formation assay

Each well of 96-well plates was coated with 50 μ L of Matrigel. Subsequently, HUVECs (1×10^4 /well) were seeded in the wells following the solidification of Matrigel. The cells in the experimental groups were treated with or without VEGF (10 ng/mL) and exposed to G4 samples at low dose (10 μ M) or high dose (20 μ M), mut samples (20 μ M), and AS1411 (10 μ M). The control groups were treated with an equal volume of serum-free ECM medium. The cells were incubated at 37 °C with 5% CO₂ for 6 h, and then images were captured using a light microscope (Nikon, Japan).

Chick embryo chorioallantoic membrane assay

The chicken embryo chorioallantoic membrane (CAM) angiogenesis model was employed to investigate the angiogenic potency of G4s. Briefly, Leghorn fertilized eggs (Pindos, Greece) were incubated for 9 days at 37 °C. Subsequently, a window was opened on the eggshell to expose the CAM, which was then covered with sterile tape, and the eggs were returned to the incubator. On the 12th day of embryo development, 100 μ L of distilled water alone (as a control) or containing G4 samples at low dose (10 μ M) or high dose (20 μ M), mut samples (20 μ M), and AS1411 (10 μ M) was applied to a 1 cm² area of the CAM inside a silicon ring. After 48 h of incubation at 37 °C, pictures were taken through a stereoscope equipped with a digital camera (Nikon, Japan), and the total area of the vessels was measured using the Image Proplus image analysis software. Each sample was tested three times, using 5–10 eggs for each data point.

NMR experiments

NMR experiments were conducted using BRUKER AVANCE 600 MHz spectrometers. Spectra were recorded at 25 °C, with RNA samples (3.1–4.2 mM) dissolved in 0.15 mL of 90% H₂O/10% D₂O, containing 10 mM sodium phosphate buffer (pH 6.8) and 100 mM KCl.

Reporting summary

Further information on research design is available in the Nature Portfolio Reporting Summary linked to this article.

Data availability

All data supporting the findings of this study are available within the paper and its Supplementary Information. Uncropped and unedited blot/gel images have been included as Supplementary data 1 and 2.

Received: 5 June 2024; Accepted: 11 March 2025;
Published online: 21 March 2025

References

- Xiao, C.-D. et al. A unique G-quadruplex aptamer: a novel approach for cancer cell recognition, cell membrane visualization, and RSV infection detection. *Int. J. Mol. Sci.* **24**, 14344 (2023).
- Byun, J. Recent progress and opportunities for nucleic acid aptamers. *Life* **11**, 193 (2021).
- Mayer, G. The chemical biology of aptamers. *Angew. Chem. Int. Ed. Engl.* **48**, 2672–2689 (2009).
- Zhu, B.-C. et al. Solution structure of a thrombin binding aptamer complex with a non-planar platinum(II) compound. *Chem. Sci.* **13**, 8371–8379 (2022).
- Ellington, A. D. & Szostak, J. W. Selection in vitro of single-stranded DNA molecules that fold into specific ligand-binding structures. *Nature* **355**, 850–852 (1992).
- Micura, R. & Höbartner, C. Fundamental studies of functional nucleic acids: aptamers, riboswitches, ribozymes and DNAzymes. *Chem. Soc. Rev.* **49**, 7331–7353 (2020).
- Zhou, J. & Rossi, J. Aptamers as targeted therapeutics: current potential and challenges. *Nat. Rev. Drug Discov.* **16**, 181–202 (2017).
- Mullard, A. FDA approves second RNA aptamer. *Nat. Rev. Drug Discov.* **22**, 774 (2023).
- Sola, M. et al. Aptamers against live targets: is in vivo SELEX finally coming to the edge? *Mol. Ther. Nucleic Acids* **21**, 192–204 (2020).
- Morita, Y., Leslie, M., Kameyama, H., Volk, D. E. & Tanaka, T. Aptamer therapeutics in cancer: current and future. *Cancers* **10**, 80 (2018).
- Courtenay-Luck N, Miller DM. AS1411: Development of an Anticancer Aptamer. In: *Therapeutic Oligonucleotides* (ed. Kurreck J). *The Royal Society of Chemistry* (2008).
- Rosenberg, J. E. et al. A phase II trial of AS1411 (a novel nucleolin-targeted DNA aptamer) in metastatic renal cell carcinoma. *Investig. N. Drugs* **32**, 178–187 (2014).
- Bates, P. J. et al. G-quadruplex oligonucleotide AS1411 as a cancer-targeting agent: Uses and mechanisms. *Biochim. Biophys. Acta Gen. Subj.* **1861**, 1414–1428 (2017).
- Yazdian-Robati, R. et al. Therapeutic applications of AS1411 aptamer, an update review. *Int. J. Biol. Macromol.* **155**, 1420–1431 (2020).
- Kotkowiak, W., Wengel, J., Scotton, C. J. & Pasternak, A. Improved RE31 analogues containing modified nucleic acid monomers: thermodynamic, structural, and biological effects. *J. Med. Chem.* **62**, 2499–2507 (2019).
- Woodruff, R. S. & Sullenger, B. A. Modulation of the coagulation cascade using aptamers. *Arterioscler. Thromb. Vasc. Biol.* **35**, 2083–2091 (2015).
- Povsic, T. J. et al. A Phase 2, randomized, partially blinded, active-controlled study assessing the efficacy and safety of variable anticoagulation reversal using the REG1 system in patients with acute coronary syndromes: results of the RADAR trial. *Eur. Heart J.* **34**, 2481–2489 (2013).
- Ganson, N. J. et al. Pre-existing anti-polyethylene glycol antibody linked to first-exposure allergic reactions to pegnivacogin, a PEGylated RNA aptamer. *J. Allergy Clin. Immunol.* **137**, 1610–1613 (2016). e1617.
- Hill RE, Hunt NT, Hirst JD. Chapter One - Studying biomacromolecules with two-dimensional infrared spectroscopy. *Adv. Protein Chem. Struct. Biol.* **93**, 1–36 (2013).
- Xiao, C. D. et al. Unusual topological RNA architecture with an eight-stranded helical fragment containing A-, G-, and U-tetrads. *J. Am. Chem. Soc.* **139**, 2565–2568 (2017).
- Xiao, C. D., Shibata, T., Yamamoto, Y. & Xu, Y. An intramolecular antiparallel G-quadruplex formed by human telomere RNA. *Chem. Commun.* **54**, 3944–3946 (2018).
- Gatto, B., Palumbo, M. & Sissi, C. Nucleic acid aptamers based on the G-quadruplex structure: therapeutic and diagnostic potential. *Curr. Med. Chem.* **16**, 1248–1265 (2009).
- Roxo, C., Kotkowiak, W. & Pasternak, A. G-quadruplex-forming aptamers-characteristics, applications, and perspectives. *Molecules* **24**, 3781 (2019).
- Bao, H. L. et al. Improving thermodynamic stability and anticoagulant activity of a thrombin binding aptamer by incorporation of 8-trifluoromethyl-2'-deoxyguanosine. *J. Med. Chem.* **64**, 711–718 (2021).
- Saha, A. et al. Nucleolin discriminates drastically between long-loop and short-loop quadruplexes. *Biochemistry* **59**, 1261–1272 (2020).
- Santos, T., Salgado, G. F., Cabrita, E. J. & Cruz, C. Nucleolin: a binding partner of G-quadruplex structures. *Trends Cell Biol.* **32**, 561–564 (2022).
- Do, N. Q., Chung, W. J., Truong, T. H. A., Heddi, B. & Phan, A. T. G-quadruplex structure of an anti-proliferative DNA sequence. *Nucleic Acids Res.* **45**, 7487–7493 (2017).
- Riccardi, C., Napolitano, E., Platella, C., Musumeci, D. & Montesarchio, D. G-quadruplex-based aptamers targeting human thrombin: discovery, chemical modifications and antithrombotic effects. *Pharmacol. Ther.* **217**, 107649 (2021).
- Kasherman, L., Liu, S. L., Karakasis, K. & Lheureux, S. Angiogenesis: a pivotal therapeutic target in the drug development of gynecologic cancers. *Cancers* **14**, 1122 (2022).
- Mi, Y. et al. Apoptosis in leukemia cells is accompanied by alterations in the levels and localization of nucleolin. *J. Biol. Chem.* **278**, 8572–8579 (2003).
- Gilles, M. E. et al. Nucleolin targeting impairs the progression of pancreatic cancer and promotes the normalization of tumor vasculature. *Cancer Res.* **76**, 7181–7193 (2016).
- Brignole, C. et al. Cell surface Nucleolin represents a novel cellular target for neuroblastoma therapy. *J. Exp. Clin. Cancer Res.* **40**, 180 (2021).
- Romano, S., Fonseca, N., Simoes, S., Goncalves, J. & Moreira, J. N. Nucleolin-based targeting strategies for cancer therapy: from targeted drug delivery to cytotoxic ligands. *Drug Discov. Today* **24**, 1985–2001 (2019).
- Christian, S. et al. Nucleolin expressed at the cell surface is a marker of endothelial cells in angiogenic blood vessels. *J. Cell Biol.* **163**, 871–878 (2003).
- Birmpas, C., Briand, J. P., Courty, J. & Katsoris, P. Nucleolin mediates the antiangiogenesis effect of the pseudopeptide N6L. *BMC Cell Biol.* **13**, 32 (2012).
- Shi, H. et al. Nucleolin is a receptor that mediates antiangiogenic and antitumor activity of endostatin. *Blood* **110**, 2899–2906 (2007).
- Iturriaga-Goyon, E. et al. AS1411 Nucleolin-specific binding aptamers reduce pathological angiogenesis through inhibition of nucleolin phosphorylation. *Int. J. Mol. Sci.* **22**, 13150 (2021).
- Birmpas, C., Briand, J. P., Courty, J. & Katsoris, P. The pseudopeptide HB-19 binds to cell surface nucleolin and inhibits angiogenesis. *Vasc. Cell* **4**, 21 (2012).
- Feng, Z., Xu, L. & Xie, Z. Receptors for respiratory syncytial virus infection and host factors regulating the life cycle of respiratory syncytial virus. *Front. Cell Infect. Microbiol.* **12**, 858629 (2022).
- Mastrangelo, P. et al. Identification of RSV fusion protein interaction domains on the virus receptor. *Nucleolin. Viruses* **13**, 261 (2021).
- Mastrangelo, P. et al. Targeting host cell surface nucleolin for rsv therapy: challenges and opportunities. *Vaccines* **5**, 27 (2017).
- Tayyari, F. et al. Identification of nucleolin as a cellular receptor for human respiratory syncytial virus. *Nat. Med.* **17**, 1132–1135 (2011).
- Pålsson, S. A. et al. Single-stranded oligonucleotide-mediated inhibition of respiratory syncytial virus infection. *Front. Immunol.* **11**, 580547 (2020).

44. Xu, Y., Ishizuka, T., Kimura, T. & Komiyama, M. A U-tetrad stabilizes human telomeric RNA G-quadruplex structure. *J. Am. Chem. Soc.* **132**, 7231–7233 (2010).
45. Joachimi, A., Benz, A. & Hartig, J. S. A comparison of DNA and RNA quadruplex structures and stabilities. *Bioorg. Med. Chem.* **17**, 6811–6815 (2009).
46. Kankia, B. Stability factors of the parallel quadruplexes: DNA versus RNA. *J. Phys. Chem. B* **123**, 1060–1067 (2019).
47. Xu, Y., Kaminaga, K. & Komiyama, M. G-quadruplex formation by human telomeric repeats-containing RNA in Na⁺ solution. *J. Am. Chem. Soc.* **130**, 11179–11184 (2008).
48. Liu, X. & Xu, Y. HnRNPA1 specifically recognizes the base of nucleotide at the loop of RNA G-quadruplex. *Molecules* **23**, 237 (2018).
49. Liu, X. et al. Structure-dependent binding of hnRNPA1 to telomere RNA. *J. Am. Chem. Soc.* **139**, 7533–7539 (2017).
50. de Silanes, I. L., d'Alcontres, M. S. & Blasco, M. A. TERRA transcripts are bound by a complex array of RNA-binding proteins. *Nat. Commun.* **1**, 33 (2010).
51. Xu, Y. et al. Finding a human telomere DNA-RNA hybrid G-quadruplex formed by human telomeric 6-mer RNA and 16-mer DNA using click chemistry: a protective structure for telomere end. *Bioorg. Med. Chem.* **22**, 4419–4421 (2014).
52. Xiao, C. D., Ishizuka, T. & Xu, Y. Antiparallel RNA G-quadruplex Formed by Human Telomere RNA Containing 8-Bromoguanosine. *Sci. Rep.* **7**, 6695 (2017).
53. Berger, C. M., Gaume, X. & Bouvet, P. The roles of nucleolin subcellular localization in cancer. *Biochimie* **113**, 78–85 (2015).
54. Fogal, V., Sugahara, K. N., Ruoslahti, E. & Christian, S. J. A. Cell surface nucleolin antagonist causes endothelial cell apoptosis and normalization of tumor vasculature. *Angiogenesis* **12**, 91–100 (2009).
55. Huang, Y. et al. The angiogenic function of nucleolin is mediated by vascular endothelial growth factor and nonmuscle myosin. *Blood* **107**, 3564–3571 (2006).
56. Otake, Y. et al. Overexpression of nucleolin in chronic lymphocytic leukemia cells induces stabilization of bcl2 mRNA. *Blood* **109**, 3069–3075 (2007).
57. Soundararajan, S., Chen, W., Spicer, E. K., Courtenay-Luck, N. & Fernandes, D. J. The nucleolin targeting aptamer AS1411 destabilizes Bcl-2 messenger RNA in human breast cancer cells. *Cancer Res.* **68**, 2358–2365 (2008).
58. Zhang, X. et al. Nucleolin phosphorylation regulates PARN deadenylase activity during cellular stress response. *RNA Biol.* **15**, 251–260 (2018).
59. Yangngam, S. et al. Cellular localization of nucleolin determines the prognosis in cancers: a meta-analysis. *J. Mol. Med.* **100**, 1145–1157 (2022).
60. Platella, C., Riccardi, C., Montesarchio, D., Roviello, G. N. & Musumeci, D. G-quadruplex-based aptamers against protein targets in therapy and diagnostics. *Biochim. Biophys. Acta Gen. Subj.* **1861**, 1429–1447 (2017).
61. Techaarpornkul, S., Collins, P. L. & Peeples, M. E. Respiratory syncytial virus with the fusion protein as its only viral glycoprotein is less dependent on cellular glycosaminoglycans for attachment than complete virus. *Virology* **294**, 296–304 (2002).
62. Griffiths, C. D. et al. IGF1R is an entry receptor for respiratory syncytial virus. *Nature* **583**, 615–619 (2020).
63. Tonello, F., Massimino, M. L. & Peggion, C. Nucleolin: a cell portal for viruses, bacteria, and toxins. *Cell. Mol. Life Sci.* **79**, 271 (2022).

64. Kulkarni, J. A. et al. The current landscape of nucleic acid therapeutics. *Nat. Nanotechnol.* **16**, 630–643 (2021).

Acknowledgements

We express our gratitude to Professor Ke Zhang at Guizhou Medical University, Guizhou, China, for generously providing the respiratory syncytial virus (RSV) used in this study. This work was supported by the National Natural Science Foundation of China (32100981, 32260141, U1812403-4-4); Ministry of Human Resources and Social Security of the People's Republic of China (201901); the Guizhou Provincial Scientific and Technologic Innovation Base ([2023]003).

Author contributions

R.-Q.T.: Investigation, Writing – Original Draft. Y.G.: Investigation. X.-H.H.: Investigation. M.-H.J., D.P. and L.-Y. F.: Data curation. X.-C.S. and S.-F.S.: provided resources and Supervision. C.-D.X.: Conceptualization, Methodology, Writing—Reviewing and Editing.

Competing interests

The authors declare no competing interests.

Additional information

Supplementary information The online version contains supplementary material available at <https://doi.org/10.1038/s42003-025-07915-1>.

Correspondence and requests for materials should be addressed to Sheng-Fa Su, Xiang-Chun Shen or Chao-Da Xiao.

Peer review information *Communications Biology* thanks Jean-Denis Beaudoin and the other anonymous reviewer(s) for their contribution to the peer review of this work. Primary Handling Editors: Jonathan Perreault and Mengtan Xing.

Reprints and permissions information is available at <http://www.nature.com/reprints>

Publisher's note Springer Nature remains neutral with regard to jurisdictional claims in published maps and institutional affiliations.

Open Access This article is licensed under a Creative Commons Attribution-NonCommercial-NoDerivatives 4.0 International License, which permits any non-commercial use, sharing, distribution and reproduction in any medium or format, as long as you give appropriate credit to the original author(s) and the source, provide a link to the Creative Commons licence, and indicate if you modified the licensed material. You do not have permission under this licence to share adapted material derived from this article or parts of it. The images or other third party material in this article are included in the article's Creative Commons licence, unless indicated otherwise in a credit line to the material. If material is not included in the article's Creative Commons licence and your intended use is not permitted by statutory regulation or exceeds the permitted use, you will need to obtain permission directly from the copyright holder. To view a copy of this licence, visit <http://creativecommons.org/licenses/by-nc-nd/4.0/>.

© The Author(s) 2025